10

Aspects of Using Chirp Excitation for Estimation of Bioimpedance Spectrum

Toivo Paavle, Mart Min and Toomas Parve
Th. J. Seebeck Dept. of Electronics
Tallinn University of Technology,
Estonia

1. Introduction

Short frequency swept signals, known as chirps, are widely used as excitation or stimulus signals in various areas of engineering as radar and sonar techniques, acoustics and ultrasonics, optical and seismological studies, but also in biomedical investigations, including bioimpedance measurement and impedance spectroscopy (Müller & Massarani, 2001; Misaridis & Jensen, 2005; Barsoukov & Macdonald, 2005; Nahvi & Hoyle, 2009).

Signal processing in the chirp-based applications is often combined with pulse compression via cross-correlation procedure and Fourier analysis. In this chapter, a similar approach is proposed for estimation of the frequency response (the impedance spectrum) of electrical bioimpedance. An advantage of the chirp-based method is that the characteristics of a biological object can be obtained in a wide frequency range during a very short measurement cycle, which nearly eliminates the influence of low-frequency biological processes (heart beating, breathing, pulsation of blood) to the result of measurement.

The changes of a spectrum monitored at sequent time intervals by means of the Fourier Transform (known as spectrogram) is an informative base for interpreting the processes in biological objects. Furthermore, the signal treatment by the cross-correlation yields a better noise immunity for the measurement system (Barsoukov & Macdonald, 2005), and adds some alternatives for estimation of the bio-impedance properties and behavior.

2. Basics of bioimpedance measurement

2.1 Object of measurement

The impedance of living tissues or, in general, of arbitrary biological matter (electrical bioimpedance, EBI) can be characterized by its electrical equivalent, which, in turn, can be represented as the frequency-dependent complex vector $\dot{Z}(j\omega) = \mathrm{Re}(\dot{Z}(j\omega)) + j\mathrm{Im}(\dot{Z}(j\omega)) = Z(\omega)\exp(j\Phi_z(\omega))$, where $\omega = 2\pi f$, $Z(\omega) = (\mathrm{Re}(\dot{Z}(j\omega))^2 + \mathrm{Im}(\dot{Z}(j\omega))^2)^{1/2}$, and $\Phi_z(\omega) = \mathrm{arctg}(\mathrm{Im}(\dot{Z}(j\omega))/\mathrm{Re}(\dot{Z}(j\omega)))$.

On the other hand, the bioimpedance is not a constant value, but a function, which is changing in time due to numerous biological processes in the living tissue, and as a matter of fact, is a function of frequency and time altogether as $\dot{Z}=Z(j\omega,t)$.

Injection of the excitation current (stimulus) $I_{exc}(t)$ with known parameters into biological object courses the response voltage $V_z(t)$, analysis of which enables to estimate the impedance spectrum $\dot{Z}(\omega)$ of the object being under the investigation.

Fig. 1 illustrates the path of excitation current through the cells of a tissue, where r_{ext} corresponds to the extracellular resistance, and the resistive components r_{int} together with intercellular capacitances C_c constitutes the intracellular impedance (Grimnes & Martinsen, 2008; Min & Parve, 2007).

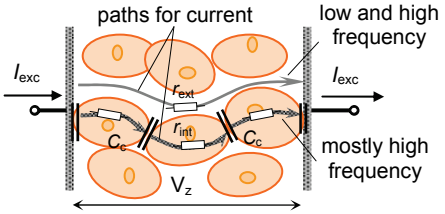

Fig. 1. Formation of the electrical bioimpedance of tissue

Very often, the response signal is analyzed using the Fourier Transform $\boldsymbol{F}(V_z(t))$ to get information about the frequency-dependent state and changes of the biological matter. Here, the impedance spectrum of EBI manifests as $\dot{Z}(j\omega)=\boldsymbol{F}(V_z(t))/\boldsymbol{F}(I_{exc}(t))$, i.e., the Fourier Transform of the response voltage determines the impedance spectrum of the object one-to-one thanks to the predetermined parameters of the excitation signal.

Usually, in theoretical considerations and simulations, the bioimpedance is substituted by a certain RC-circuit. Naturally, the accuracy of such approximation depends on the number and configuration of components. In Fig. 2a, a 5-element circuit is shown, where R_0 corresponds to the extracellular resistance r_{ext} of a tissue, while R_1, C_1, R_2 and C_2 stand for the intracellular parameters. The respective Bode diagram has two real poles f_{p1}, f_{p2}, and two zeros f_{z1}, f_{z2} (Fig. 2b), spread typically over the frequency range from some kHz up to several MHz (Nebuya *et al* 1999; Pliquett *et al*, 2000; Grimnes & Martinsen, 2008).

The Laplace transform of the 5-element EBI (Fig. 2a) can be expressed as (Paavle *et al* 2008)

$$Z(s)=\frac{R_0(1+sC_1R_1)(1+sC_2R_2)}{R_0\left[sC_2(1+sC_1R_1)+sC_1(1+sC_2R_2)\right]+(1+sC_1R_1)(1+sC_2R_2)} \tag{1}$$

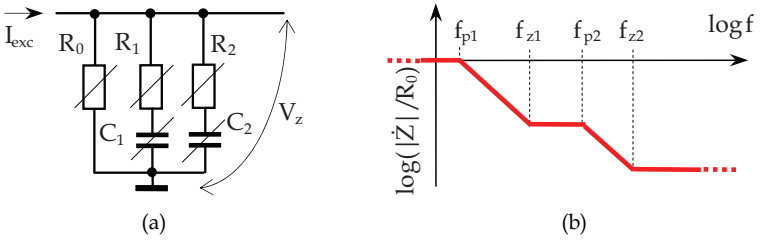

Fig. 2. (a) 5-element model and (b) Bode diagram of the bioimpedance

In the simplest case, where $C_2 \rightarrow 0$ (basic 3-element EBI):

$$Z(s) = \frac{R_0(1 + sC_1R_1)}{1 + sC_1(R_0 + R_1)} \tag{2}$$

For adequate estimation of the bioimpedance, the spectrum of excitation signal should cover the frequency range of the object $\dot{Z}$ as much as possible. For that reason, several types of broadband excitation signals (e.g., Maximal Length Sequence (Gawad *et al*, 2007), multisine (Sanchez *et al* 2011)) are preferable. However, in this chapter, we will focus on the use of chirp excitation due to several advantages of it: wide and flat amplitude spectrum (Nahvi & Hoyle, 2009) together with independent scalability in the time and frequency domain.

2.2 Essential of chirp excitation

2.2.1 Variety of chirps

A sine-wave based chirp with current phase $\theta(t)$ can be described mathematically as

$$V_{\mathrm{ch}}(t) = A\sin\left(\theta(t)\right) = A\sin\left(2\pi\int f(t)\mathrm{d}t\right) \tag{3}$$

where A is the amplitude, and $f(t) = (\mathrm{d}\theta(t)/\mathrm{d}t)/2\pi$ is instantaneous frequency of the chirp signal.

A definite class of chirps has the instantaneous frequency $f(t)$, which changes accordingly to some power function of the n^{th} order (power chirps). Their specific quantity is chirping rate $\beta=(f_{\mathrm{fin}}-f_{\mathrm{st}})/T_{\mathrm{ch}}^{n}$, where f_{st} and f_{fin} are the initial and final frequencies, respectively, and T_{ch} is the duration of the pulse. Chirps of this type can be expressed as

$$V_{\mathrm{ch}}(t) = A\sin\left(2\pi\left(f_{\mathrm{st}}t + \beta t^{n+1}/(n+1)\right)\right) \tag{4}$$

The instantaneous frequency of a chirp can be increasing (up-chirps, $\beta>0$) or decreasing (down-chirps, $\beta<0$) quantity. Besides, sometimes it is practical to generate chirps with a symmetrical bidirectional frequency change (bidirectional or double chirps). In this case, the actual duration of the pulse is $2T_{\mathrm{ch}}$, and the sign of chirping rate alters at $t = T_{\mathrm{ch}}$, causing mirrored waveform of the pulse against that moment.

Fig.3 sketches waveforms of different chirps with the equal pulse duration and almost equal frequency range. A very basic linear (n=1) chirp with f_{st}=0 can be described in accordance with the expression (4) as $V_{\mathrm{ch}}(t)=A\sin(2\pi f_{\mathrm{fin}}t^2/2T_{\mathrm{ch}})$. It is depicted in Fig. 3a.

Fig. 3b shows the waveform of quadratic (n=2) down-chirp. However, the rule of frequency change can be arbitrary. For example, in some specific measurements, excitation with the exponential chirping rate $\beta = (f_{\mathrm{fin}}/f_{\mathrm{st}})^{t/T\mathrm{ch}}$ is appropriate (Darowicki & Slepski, 2004). The waveform of sinusoidal exponential chirps (see Fig. 3c) is described as

$$V_{\mathrm{ch}}(t) = \sin\left(2\pi f_{st}T_{\mathrm{ch}}(\beta - 1)/\ln(\beta)\right) \tag{5}$$

Generation of a perfect sine-wave chirp requires quite complicated hardware, which can cause problems, especially in on-chip solutions. That is why so-called signum-chirps (known also as pseudo-, binary- or Non-Return-to-Zero (NRZ) chirps) are often implemented (Figs. 3d and 3e; the latter one depicts a binary chirp with bidirectional change

of frequency). This kind of chirps can be defined by the signum-function of respective sine-wave chirps as $V_{ch}(t)=V_{sgn}(t)=\text{sign}(V_{sin}(t))$, which have binary values $+A$ and $-A$ only.

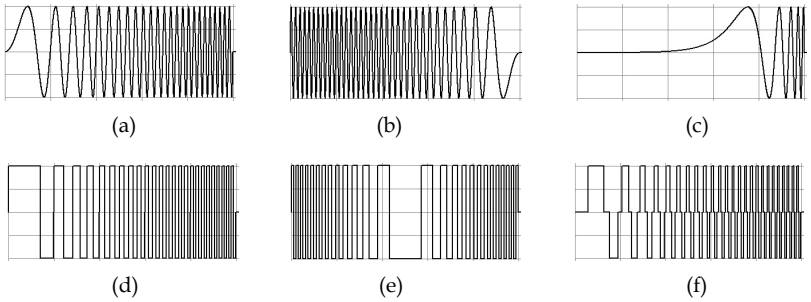

Fig. 3. Examples of chirp waveforms with the equal maximal frequency and duration, $V_{ch}(t)$ vs. time: (a) linear sine-wave chirp; (b) quadratic down-chirp; (c) exponential chirp; (d) signum-chirp; (e) signum-chirp with bidirectional (down-up) run of frequency; (f) ternary chirp with shortened duty cycle by 30°

Rectangular waveforms simplify signal processing: both generation of excitation and processing of the response will be substantially simpler. Especially simple is calculating of the correlation function or deconvolution in the time domain – shifting and multiplication with a reference signal having only {+1, -1}, or {+1, 0, -1} values (Rufer *et al*, 2005).

Additional advantage of signum-chirps is their unity crest factor (i.e., the peak amplitude ratio to the root-mean-square (RMS) value of the signal), and major energy compared with the sine-wave chirps of the same length. Unfortunately, using of rectangular signals causes the worse purity of the spectrum due to the accompanying higher harmonic components.

Suppression of the particular harmonic component in the spectrum of rectangular signals can be achieved by shortening the duty cycle of the signal by a certain degree α_d per every quarter-period (Parve & Land, 2004). Signum-chirps, modified in this way, are called Return-to-Zero (RZ) or ternary chirps. It means that $V_{sgn}(t)$ returns to zero, if the value of current phase falls into the intervals $2n\pi-\alpha_r<\theta(t)<2n\pi+\alpha_r$ or $(2n+1)\pi-\alpha_r<\theta(t)<(2n+1)\pi+\alpha_r$, where $\alpha_r=\pi\alpha_d/180$ in radians, and n=0, 1, 2, … (Fig. 3f). For explanation let us remember that spectra of a rectangular signal can be declared as the Fourier series of odd harmonics:

$$\boldsymbol{F}(\omega t)=\frac{4A}{\pi}\left[\frac{\cos\alpha_r}{1}\sin\omega t+\frac{\cos 3\alpha_r}{3}\sin 3\omega t+\ldots\right]=\frac{4A}{\pi}\left[\sum_{i=1}^{\infty}\frac{\cos(2i-1)\alpha_r}{2i-1}\sin(2i-1)\omega t\right] \quad (6)$$

It follows from (6) that the k^{th} harmonic (k=2i–1, and i=1, 2, 3, …) is absent from the series $\boldsymbol{F}(\omega t)$, when $k\alpha_r=\pm(2n+1)\pi/2$, and n=0, 1, 2, … , because of $\cos(k\alpha_r)=0$. Consequently, in the case of $\alpha_r=\pi/6$, the $(3+6n)^{th}$ harmonics are removed, and for $\alpha_r=\pi/10$, the $(5+10n)^{th}$ harmonics are removed, etc. (Paavle et al, 2007).

2.2.2 Short-time chirps (titlets)

Commonly, referring to chirps, signals of many cycles (rotations by 2π of the chirp generating vector) are considered (multi-cycle chirps). It does not need to be so, and the

chirps with a single cycle or even less ($\theta(T_{ch}) \le 2\pi$) can be generated and used, too. For such kind of ultra short chirps, the neologism "titlets" or Minimal Length Chirps (MLC) have been used (Min et al, 2011a).

The titlets can be very effective excitation signals in applications, where broadband excitation is necessary, but the minimal power consumption or extremely fast measurement are required at the same time. Because of the prospective use of titlets, a special attention to their properties will be paid below. The diagram in Fig. 4 explains the forming of a single-cycle linear sine-wave chirp.

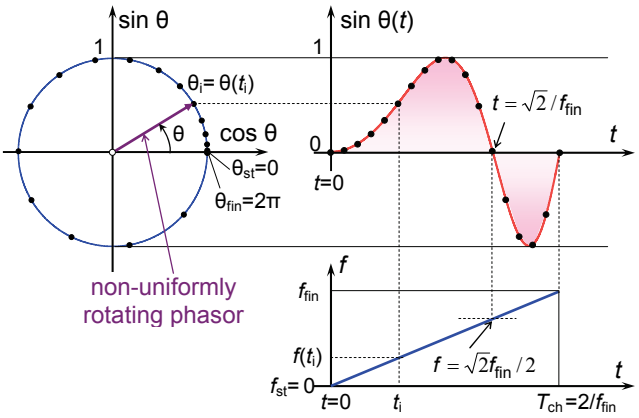

Fig. 4. Genesis of the linear single-cycle sine-wave chirp

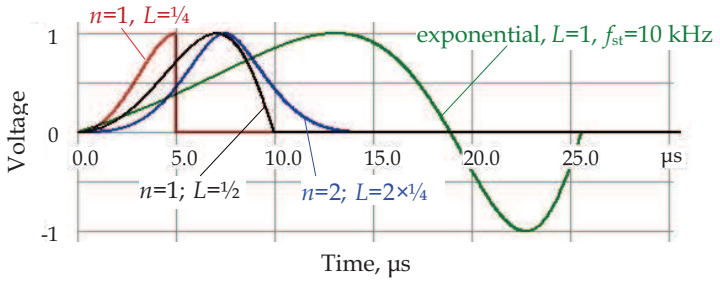

Fig. 5. Examples of titlet waveforms with f_{fin}=100 kHz (f_{st}=0 for power titlets)

Considering (4), we can state that the equality of phases $\theta(t) = 2\pi(f_{st}T_{ch}+\beta T_{ch}/(n+1) = 2\pi L$ is valid for the $t = T_{ch}$. Thereby, the number of cycles L can be an integer or fractional quantity. It allows us to derive the relationship between the length of the chirp and its parameters. For the n^{th} order power chirps this relationship expresses as (Min *et al*, 2011a)

$$T_{ch} = L(n+1)/(nf_{st} + f_{fin}) \tag{7}$$

Thus, for the single-cycle linear chirp with f_{st}=0, the pulse duration $T_{ch}=2/f_{fin}$. It follows for this case that the change of polarity ($\theta(t) = \pi$) occurs at $t = \sqrt{2} / f_{fin}$, while the instantaneous frequency is $f = \sqrt{2} f_{fin} / 2$ (see Fig. 4).

Similarly, considering (5), one can show that for exponential chirps the duration of a pulse is

$$T_{ch} = L \cdot \ln\left(f_{fin} / f_{st}\right) / \left(f_{fin} - f_{st}\right) \tag{8}$$

Simulated waveforms of some typical titlets with $L \leq 1$ are shown in Fig. 5.

2.3 Signal analysis and bioimpedance measurement by using Fourier Transform

Spectral analysis is the irreplaceable method as for the study of the behavior of excitation signals in the frequency domain as well as for processing the response signal in the bioimpedance measurements.

It is obligatory to remember that in the modeling and processing of chirp signals the selected sampling rate f_s must follow the Nyqvist criterion over the whole frequency range, i.e., the condition $f_s \geq 2f_{fin}$ must be fulfilled. The sampling rate determines the total number of samples N_{ch} during a chirped pulse as $N_{ch} = T_{ch} f_s$. Yet, the simulation or real processing time T_{tot} can be longer than T_{ch}. In this case, the zero padding is used at $t > T_{ch}$. The length of the input array for the Fast Fourier Transform (FFT) is $N = T_{tot} f_s \geq N_{ch}$, and it determines the frequency resolution Δf (difference between two successive frequency bins) of the FFT processing, whereas $\Delta f = f_s / N$ according to the uncertainty principle (Vaseghi, 2006). The acquired positive frequency range of the FFT processing in Hz is 0, …, $N\Delta f/2$ by steps of Δf.

2.3.1 Principles of bioimpedance measurements

There are several methods to calculate the frequency spectrum of the bioimpedance response. A typical way is the implementation of two FFT-channels for the response and excitation signals separately (Min *et al*, 2011a). Nevertheless, in the following discussion we will focus mainly on the structure and modeling of a specific bioimpedance measurement system, which incorporates the cross-correlation procedure together with following FFT-processing (Paavle *et al*, 2008, Min *et al*, 2009, see Fig. 6).

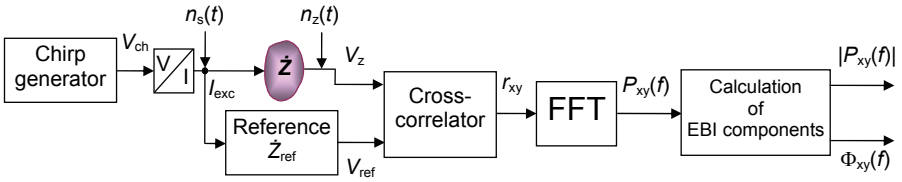

Fig. 6. Basic structure of the measurement system

In such a system, the cross-correlation function (CCF) is calculated: (a) between the response $V_z(t)$ and excitation $V_{ch}(t)$ at the unity gain in the reference channel ($V_{ref}(t) = V_{ch}(t)$, $\dot{Z}_{ref} = 1$), or (b) between the response and predefined reference signal $V_{ref}(t)$ (reference channel includes the known impedance $\dot{Z}_{ref} \neq 1$). In the latter case, the system works as the matched filter, enabling detection of mismatches between the impedance vectors $\dot{Z}$ and $\dot{Z}_{ref}$ more precisely together with somewhat better noise reduction. The source noise $n_s(t)$ and object noise $n_z(t)$ can be taken into account in simulations as shown in Fig. 6.

In general, calculation of the CCF proceeds as

$$r_{xy}(\tau) = Corr\left(V_z(t), V_{ref}(t)\right) = \overline{V_z(t) V_{ref}(t+\tau)}, \tag{9}$$

where τ is a variable delay (lag) and the overline denotes averaging.

Using broadband chirp excitation, the waveform $r_{xy}(\tau)$ of CCF is similar to the $\sin(x)/x$ type sinc-function affected by the nature of $V_z(t)$ and is strongly compressed close to $\tau = 0$.

The CCF includes both the information about the amplitude level and phase shift of the bioimpedance vector. Thanks to this fact, only a single FFT-block is necessary to obtain the complete information about the object. Otherwise, when using the direct Fourier Transform of the response, another FFT channel is required to establish the basis for phase evaluations.

In accordance with the cross-correlation theorem (generalized Wiener-Khinchin theorem), the correlation function is equivalent to the inverse Fourier Transform of the complex cross-power spectrum density $P_{xy}(f)$ with the magnitude and phase spectral components $\left|P_{xy}(f)\right| = \sqrt{(\mathrm{Re}(P_{xy}(f)))^2 + (\mathrm{Im}(P_{xy}(f)))^2}$ and $\Phi_{xy}(f)$=arctg(Im($P_{xy}(f)$)/ Re($P_{xy}(f)$)), respectively (Vaseghi, 2006). Thereby, the phase component $\Phi_{xy}(f)$ specifies the phase difference between the vectors V_z and V_{ref}, and magnitude presents the geometric mean of the power spectral densities of the signals $V_z(t)$ and $V_{ref}(t)$ (McGhee *et al*, 2001).

2.3.2 Modeling of the measurement system

Accordingly to the main architecture of measurement system (Fig. 6) and model of EBI (Fig. 2a), a special PC-model (Fig. 7) was developed for verifying the theoretical conceptions (Paavle *et al*, 2008).

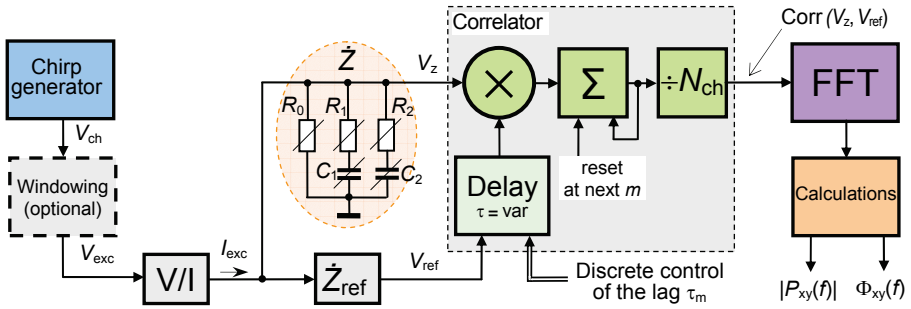

Fig. 7. Model of the measurement system

The cross-correlation function is calculated by the cumulative adder for every m^{th} lag τ_m as

$$r_{xy}[m] = \frac{1}{N_{ch}} \sum_{k=0}^{N_{ch}-1} V_z[k] \cdot V_{ref}[k + \tau_m], \tag{10}$$

where $k = 0 \ldots N_{ch}-1$, and N_{ch} is the number of samples per length of the chirp pulse (McGhee *et al*, 2001).

If the uniform delay step is $\Delta\tau$, then for the overall delay interval (observation time) $t_{obs} = \tau_{max} - \tau_{min}$ ($\tau_{min} \le \tau_m \le \tau_{max}$) the number of necessary computing cycles is $M + 1$ with $M = t_{obs}/\Delta\tau$. As a result, we acquire an array of correlation values $r_{xy}[m]$ with $m = 0 \dots M$. Supposing that the selected $\Delta\tau$ and τ_{min} are integer multiples of the sampling interval $1/f_s$, the m^{th} delay expresses as $\tau_m = f_s(\tau_{min} + m\Delta\tau)$.

In the following Fourier Transform, the array r_{xy} of length $M+1$ represents the input stream for the FFT-block, while in accordance with the uncertainty principle (see above), the frequency resolution of spectra becomes $\Delta f = 1/t_{obs}$ over the frequency range $f = 0 \dots 1/(2\Delta\tau)$.

3. Spectral features and energy of chirps

Next, let us take a look at the results of direct Fourier Transform of distinct chirp pulses. The direct FFT of different excitation signals enables to compare their amplitude and power spectra together with estimation of the energy properties keeping in view the requirements for the bioimpedance measurement.

Important and desired spectral properties of excitation signals to improve the quality of wideband measurement are:

- flat amplitude spectrum with minimal fluctuation (ripple) together with the absence of overshoots inside the generated (excitation) bandwidth $B_{exc} = f_{fin} - f_{st}$;
- steep drop-down of the amplitude spectrum outside the bandwidth B_{exc};
- maximal energy-efficiency, i.e., the ratio between the energy lying within the generated (excitation) bandwidth B_{exc} and total energy of the signal.

For some specific applications, these properties must coincide with minor power consumption and with shortness of signal to ensure quick measurement.

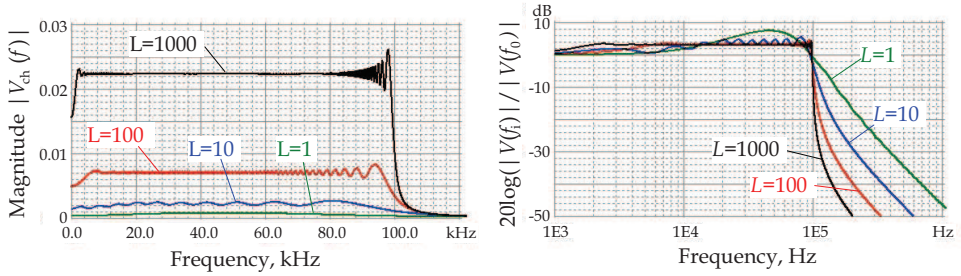

Fig. 8. Voltage spectral density of linear chirps 0…100 kHz (Δf=50 Hz): (a) linear scaling at the unity amplitude of chirp pulses; (b) normalized logarithmic scaling

Fig. 8 depicts the amplitude spectra of linear sine-wave chirps of different length in the linear and in the normalized logarithmic scales. Thereby, the base of normalizing is the amplitude $|V(f_0)|$, i.e., the magnitude at the lowest frequency bin f_0 of the Fourier Transform. It is obvious that long chirps assure the more fitting shape of spectra, except a certain rippling caused by the Gibbs effect. The latter can be suppressed by using a kind of windowing in the time domain (often a boxcar-type window function is used for this purpose), but in this case, the total energy of the signal decreases.

Fig. 9 shows the frequency run and respective amplitude spectra of different titlets. It appears that the desired shape of the spectrum, including flatness, satisfying drop-down outside the bandwidth (slopes from –20 dB/dec to –80 dB/dec were observed) and admissible overshoots can be achieved by a proper selection of the type and length of titlet. Moreover, additional correction and shaping of spectra can be attained by windowing of titlets in the time domain (see below in Sect. 3.2). In Fig.10, waveforms and amplitude spectra of some rectangular chirps (see Sect. 2.2.1) with L=10 are shown. Naturally, for this kind of chirps, the rippling of spectra is noticeable.

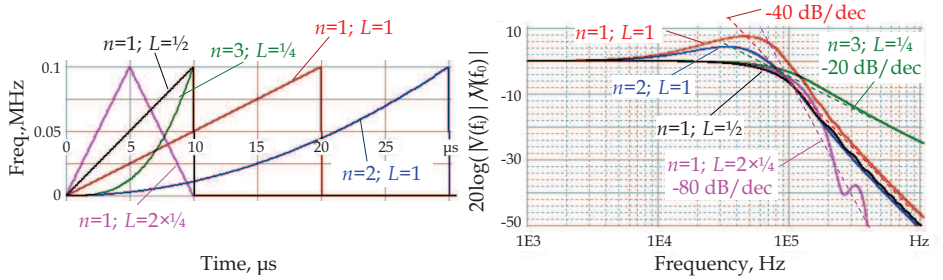

Fig. 9. (a) Frequency run and (b) amplitude spectra of different titlets with B_{exc}=0…100 kHz

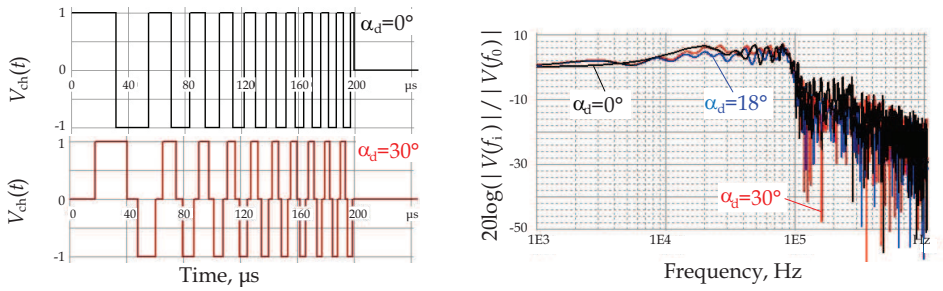

Fig. 10. (a) Waveforms of binary and ternary chirps with α_d=30°; (b) amplitude spectra of binary and ternary chirps with α_d =30° and α_d =18° (Δf=100 Hz)

3.1 Energy of chirps

3.1.1 Sine-wave chirps

In principle, the total energy of a chirp signal at the unity load (R_{load}=1Ω) expresses in time domain as

$$E_{tot} = \int_0^{T_{ch}} V_{ch}(t)^2 dt \,, \tag{11}$$

which leads to $E_{tot} = (A^2/2)T_{ch}$ for the long term chirps of sinusoidal waveform.

According to the Parseval's theorem, the total energy in the frequency domain is the same as the energy in the time domain (Vaseghi, 2006). For chirps with the finite length, a certain

part of signal energy falls outside the useful (generated) bandwidth caused by higher frequency components. For that reason, it is necessary to distinguish the total energy of a generated chirp pulse, which varies proportionally with T_{ch}, and the useful energy E_{exc}, falling inside the chirp bandwidth B_{exc}. Typically, $E_{exc} < E_{tot}$, while absolute values of both quantities depend on the chirp length, waveform and spectral nature. To characterize the percentage of the useful energy, we employ the term of energy-efficiency as $\delta_E = E_{exc}/E_{tot}$. For sine-wave chirps with $L \to \infty$ the ratio $\delta_E \to 1$.

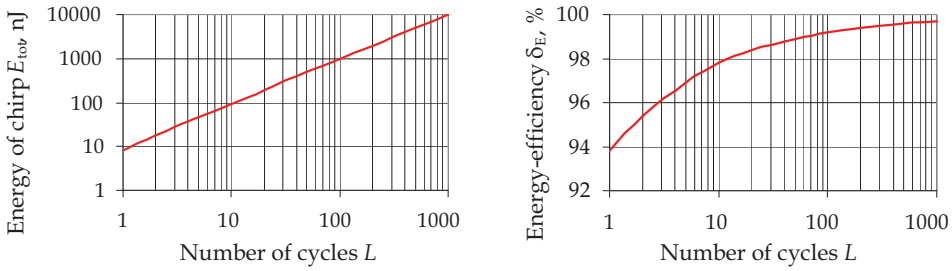

Fig. 11. (a) Total energy and (b) energy-efficiency of linear sine-wave chirps

Type of chirp (titlet)	L	f_{st}, Hz	T_{ch}, μs	P_{avg}, mW	E_{tot}, nJ	δ_E, %
linear	¼	0	5.0	0.32	1.6	55.0
	½	0	10.0	0.38	3.8	90.6
	1	0	20.0	0.41	8.3	93.5
	10	0	200.0	0.47	94.4	97.8
	100	0	2000	0.49	982	99.3
quadratic	½	0	15.0	0.29	4.4	93.9
	1	0	30.0	0.33	10.0	95.7
	100	0	3000	0.464	1393	99.5
cubic	1	0	40.0	0.28	11.1	96.4
exponential	1	1	115.1	0.135	15.6	97.8
	10	1	1151	0.235	271	99.5
double-quadratic	2×¼	0	2×7.5	0.23	3.4	93.1
NRZ signum-chirp	1	0	20.0	1.0	20.0	84.1
	1000	0	20e3	1.0	20e3	85.1
RZ chirp (18° short.)	1000	0	20e3	0.8	16.0e3	93.1
RZ chirp (30° short.)	1000	0	20e3	0.67	13.3e3	92.1

Table 1. Energy and average power of different chirp pulses with $f_{st} \approx 0$ and f_{fin}=100 kHz

Considering expressions (11) and (4) or (5), the analytical description of the chirp energy becomes very complicated. So it is reasonable to calculate the respective quantities numerically. Nevertheless, a good approximation of total energy and energy-efficiency of arbitrary chirp signal can be obtained using the results from the Fourier Transform as follows (Paavle *et al*, 2010):

$$\delta_E = \sum_{i=N_{st}}^{N_{fin}} |V_{ch}(f_i)|^2 \Big/ \sum_{i=0}^{N_{max}-1} |V_{ch}(f_i)|^2 \tag{12}$$

where $|V(f_i)|$ is the value of the amplitude spectrum at i^{th} frequency bin, N_{st} and N_{fin} are the numbers of frequency bins, corresponding to the f_{st} and f_{fin}, respectively. N_{max} is the total number of frequency bins, and the divisor in (12) corresponds to the total energy E_{tot}. Of course, this method enables to calculate the partial energy for any frequency interval inside the range of 0 to $N_{max}\Delta f$.

The curves in Fig. 11 present the dependence of the energy and energy-efficiency of linear sine-wave chirps on the number of chirp cycles graphically. A selection of power and energy parameters for different chirps and titlets, obtained from the FFT-processing by using the expression (12), are converged into Table 1, where the average power $P_{avg} = \frac{1}{T_{ch}} \int_0^{T_{ch}} V_{ch}(t)^2 dt = E_{tot} / T_{ch}$ presumes the 1 kΩ load.

3.1.2 Binary signum-chirps

A specific feature of signum-chirps is the gradually decreasing amplitude spectrum by step width of $2B_{exc}$ as shown in Fig. 12 (Min *et al*, 2009). Let us analyze this phenomenon.

The fundamental harmonic of a regular rectangular signal with amplitude $A_1 = (4/\pi)\,A$ has a root-mean-square (RMS) value $A_1/\sqrt{2} = 4A/(\pi\sqrt{2})$, energy $E_1 = (A_1^2/2)\,T_{ch} = (8/\pi^2)\,A^2\,T_{ch}$, and power $W_1 = E_1/T_{ch} = (8/\pi^2)\,A^2$, which creates a constant value power spectral density (PSD) $w_1 = W_1/B_{exc}$, V²/Hz, within the bandwidth B_{exc} of fundamental harmonic:

$$w_1 = \left(8/\pi^2\right) A^2 / B_{exc} \tag{13}$$

The amplitudes of k^{th} higher harmonics are of $A_k = A_1/k$. Therefore, the power of every k^{th} higher odd harmonic (k =3, 5, 7, …) is equal to W_1/k^2, being spread over the frequency range $B_k = kf_{fin} - kf_{st} = kB_{exc}$. Due to the fact that higher harmonics have k times wider bandwidth than the fundamental (first) harmonic has, the PSD for higher harmonics can be expressed through (12) as $w_k = (w_1/k^2)/k = w_1/k^3$ (Min *et al*, 2009).

The total power of generated signal $V_{ch}(t)$ is gradually distributed over its whole frequency range, theoretically from f_{st} to ∞, see Fig. 12. The PSD p_h of every gradual h^{th} level (h= 1, 2, 3, 4, …) of the spectrum, beginning from the first one p_1, is the sum of power spectral densities of the fundamental and higher harmonics, w_1 and w_k, which contribute into the given level h. Into the PSD p_1 of the first level contribute all the signal components $p_1 = w_1 + w_3 + w_5 + w_7 + \ldots$, but into the second level mere the higher harmonics $p_2 = w_3 + w_5 + w_7 + \ldots$, ($k$ = 3, 5, 7, …), and into the third level only the harmonics beginning from k = 5, $p_3 = w_5 + w_7 + \ldots$, etc.

Generally,

$$p_h \approx w_1 \sum_{i=h}^{h+m} (2i-1)^{-3} \tag{14}$$

in which i is an integer beginning from h, that is: $i = h$, (h+1), (h+2), (h+3), …, (h+m), where m is the number of higher odd harmonics taken into account.

The partial power $P_1 = p_1 B_{exc} = P_{exc}$ of the first level (h=1) is the useful excitation power

$$P_{exc} \approx W_1 \sum_{i=h}^{1+m} (2i-1)^{-3} \tag{15}$$

The power P_{out} falling outside B_{exc} is lost. The lost power can be found as a summed up power of higher harmonics within the next levels of spectrum (h= 2, 3, 4, etc., see Fig. 10):

$$P_{out} \approx W_1 \sum_{i=1}^{1+m} 2(i-1)/(2i-1)^3 \tag{16}$$

where $W_1 = w_1 B_{exc}$ in (15) and (16) is the power of fundamental harmonic. As the minimal frequency for every level is kf_{st}, then the equations (14-16) are approximate ones, which become absolutely exact only for f_{st}=0. In practice, when the excitation bandwidth B_{exc} exceeds one decade significantly, e.g., $f_{fin} / f_{st} > 30$, these equations are exact enough for engineering calculations.

The total chirp energy is $E_{tot} = E_{exc} + E_{out} = (P_{exc} + P_{out})\, T_{ch}$ and the useful excitation energy in it is $E_{exc} = P_{exc}\, T_{ch}$. From (15) and (16) follows the role of useful energy $\delta_E = E_{exc} / E_{tot}$. Considering f_{st}=0, the ratio for the energy-efficiency expresses as

$$\delta_E = \left(\sum_{i=1}^{\max h} (2i-1)^{-3} \right) / \left(\sum_{i=1}^{\max h} (2i-1)^{-2} \right) \tag{17}$$

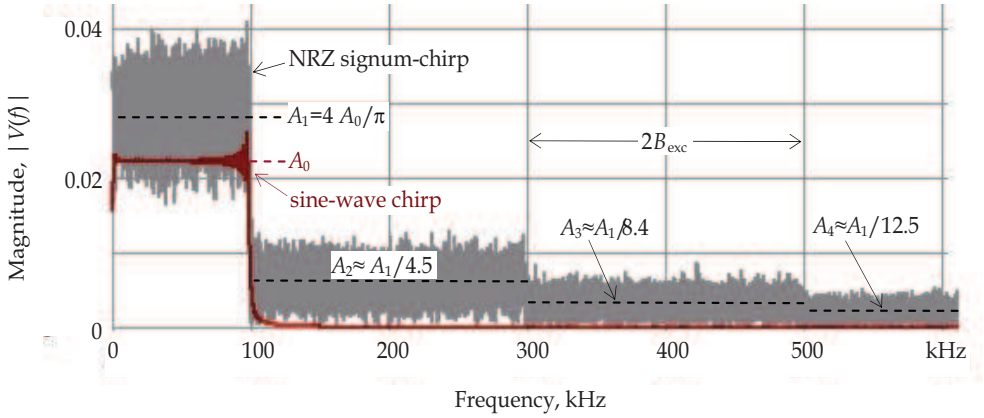

Fig. 12. Amplitude spectra of 1000-cycles sine-wave chirps and signum-chirps with f_{st}=0 and f_{fin}=100 kHz (A=1)

Taking into account all the higher harmonics ($m \to \infty$ and $(\max h) \to \infty$), the sums in (17) will obtain limit values, which can be found via Riemann zeta function (Dwight, 1961):

$$\zeta(x) = \sum_{n=1}^{\infty} n^{-x} \tag{18}$$

Riemann's mathematics gives us the following limit values for the sums in (17):

$$\sum_{i=1}^{\infty}(2i-1)^{-2}=\pi^2/8\,, \tag{19}$$

$$\sum_{i=1}^{\infty}(2i-1)^{-3}=7\zeta(3)/8\,, \tag{20}$$

where $\zeta(3)\approx1.202$ is termed the Apéry's constant (Dwight, 1961). Now, using equations (19) and (20), we can express the part of useful energy in the linear NRZ signum-chirp pulse as

$$\delta_E=7\zeta(3)/\pi^2 \tag{21}$$

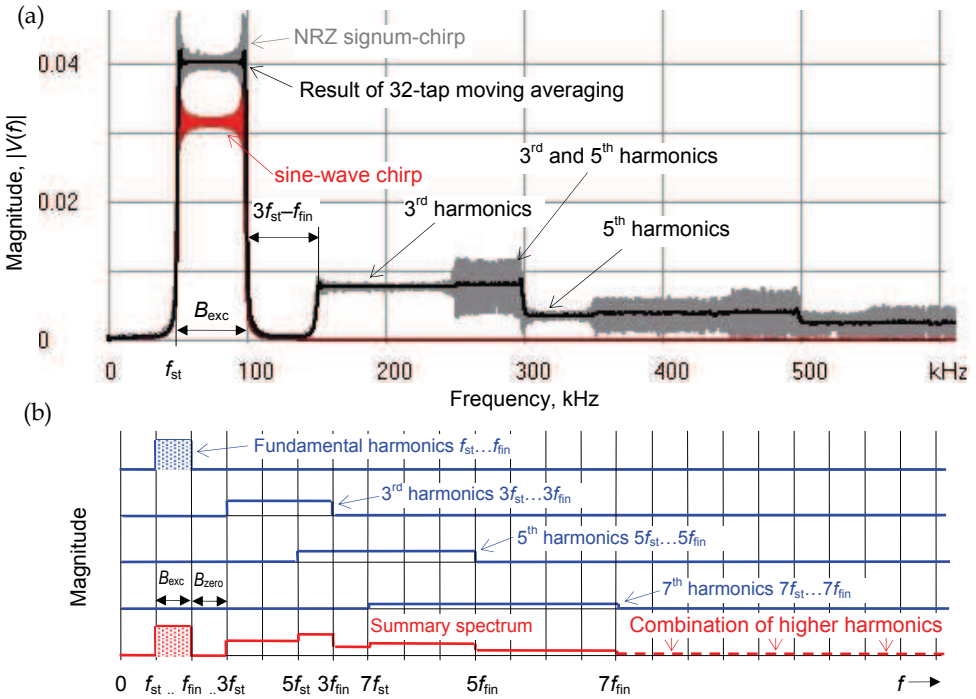

Fig. 13. (a) Amplitude spectrum of signum-chirp with f_{st}=50 kHz and f_{fin}=100 kHz (A=1; L=1000); (b) explanatory diagram of forming the amplitude spectrum at $f_{st}\neq0$

When f_{fin} / f_{st} >> 30 and m >> 1, the value of δ_E = 0.852 and the spectrum has practically uniform energy distribution over the B_{exc}. The relative decrement of every h^{th} step of the averaged amplitude can be calculated from (14) as $\delta_h=(E_{exc}/E_h)^{1/2}=A_1/A_h$. The values for some lower order levels are $\delta_2\approx4.51$, $\delta_3\approx8.44$, and $\delta_4\approx12.47$ – see the approximations given in Fig. 12. For the next levels, a rough approximation $\delta_h\approx4(h-1)+1$ is appropriate for engineering calculations (Min *et al*, 2009).

The shape of amplitude spectrum becomes more complicated, if the initial frequency $f_{st} \neq 0$. Though, the spectrum retains the gradual character, the levels do not attenuate monotonically. An example of this kind of spectrum is shown in Fig. 13a, where f_{st}= 50 kHz and f_{fin}=100 kHz. In general, the height and location of spectral levels can be various, depending on the ratio between f_{st} and f_{fin}.

The forming of spectra as the sum of its harmonic components is explained by the draft diagram in Fig. 13b. Fulfillment of the condition $3f_{st} > f_{fin}$ produces the frequency area $B_{zero} = 3f_{st} - f_{fin}$ next to the excitation bandwidth, where the spectrum has almost zero amplitude. In this particular case, the spectral density within the excitation bandwidth is determined only by the fundamental harmonics from f_{st} to f_{fin}. It can be shown, considering the Eqs.(13) –(16), that here the energy-efficiency $\delta_E = 8/\pi^2$.

3.1.3 Ternary chirps

Caused by the absence of particular harmonics (see Sect. 2.2.1), the position and span of amplitude levels of ternary chirps (RZ chirps) differ from the levels of the respective binary chirp. Fig. 14a enables to compare the amplitude spectra of several rectangular chirps with L=1000 at various durations of the zero-level state α_d (shortening).

Let us pay attention to the changed stretch of the amplitude levels. For example, in the case of $\alpha_d = 30^o$, the average amplitude of 2nd level (h=2) stretches uniformly from f_{fin} up to the $5f_{fin}$. As the 3rd harmonic are absent, this 2nd level is formed by the amplitudes of the 5th and higher harmonics up to the frequency $5f_{fin}$.

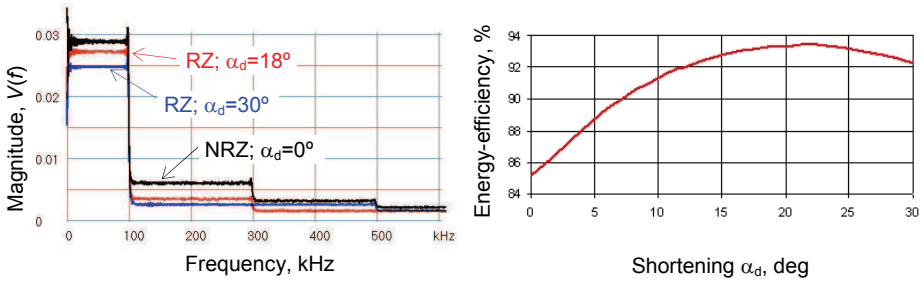

(a) (b)

Fig. 14. (a) Amplitude spectra of ternary chirps with f_{fin}=100 kHz (32-tap moving averaging has been applied for smoothing); (b) energy-efficiency of ternary chirps vs. zero-level state (shortening)

Average power of ternary chirps is less than it of respective binary chirps, but the percentage of their useful energy is surprisingly high – over 90% mostly (see also Table 1). Actually, it is possible to generate ternary chirps with any value of the zero-state, but only a few values produce the removing of particular harmonics (see Eq. 6 in Sect. 2.2.1). Nevertheless, we can analyze the energy properties of arbitrary ternary chirp. Employing the equation (12), the maximal energy-efficiency $\delta_E \approx 93.4\%$ was observed at $\alpha_d \approx 22.5^o$, which does not cause disappearance of any odd harmonic component. Dependence of the energy-efficiency on the shortening α_d is plotted in Fig. 14b.

3.2 Windowing of chirps

In the use of some short-time chirps, the problem of flatness of the amplitude spectrum arises (see Fig. 9b). For the single-cycle sine-wave chirp, the maximum overshoot of normalized voltage spectral density is about +7.4 dB inside the chirp bandwidth. To improve the flatness of spectrum, a kind of additional windowing of chirp pulses should be used (in fact, every finite chirp pulse can be dealt as one inside the rectangular window, however we consider this case as the unwindowed one). As a rule, the windowing accompanies with some loss of total energy and power of signals, but still the δ_E can be rather high. On the other hand, frequently the spectral density attains steeper drop-off outside the chirp bandwidth due to windowing. Hence, the optimal choice of windows presumes a certain trade-off always.

In this work, several typical (Hanning, Hamming, Nuttall, etc.) and some specific window functions $F_{win}(t)$ were under study (Barsoukov & Macdonald, 2005). For example, a convenient shaping of amplitude spectra was achieved by implementing window functions $F_{win}(t)=\sin^2(\pi t / T_{ch})$, which can be dealt as a particular case of the Tukey window with the squared-sine lobes and with the tapering time $T_{ch}/2$. Almost perfect shaping was attained using a non-symmetrical windowing in the form of $F_{win}(t)=(t/T_{ch})^a$ with the selectable exponent a (usually a =2…8) (Paavle *et al*, 2010). Some windowing results both in the time and frequency domain are shown in Fig. 15.

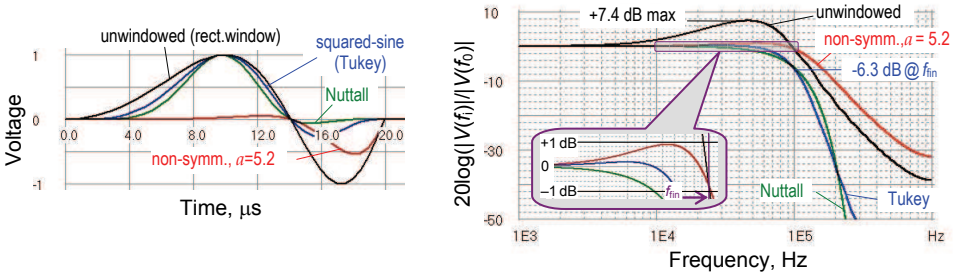

(a) (b)

Fig. 15. Effect of windowing to the single-cycle sine-wave chirp, f_{st}=0, f_{fin}=100 kHz, T_{ch}=20 μs: (a) windowed waveforms; (b) normalized spectra of the windowed waveforms

Usually, the deviation about ± 3 dB of the amplitude spectrum inside the B_{exc} is considered as satisfactory for spectral flatness. There are several ways to achieve such the requirement. Using the non-symmetric windowing makes the deviation even less than ± 1 dB accessible (see Fig.15b), but the quantity of useful energy reduces noticeably due to the plain slope of the spectrum at $f > f_{fin}$: for the case, as shown in Fig. 15, the energy-efficiency δ_E=73.1% was observed in simulations. Substantially higher δ_E was achieved by using of Nuttall (δ_E=92.3%) and Hanning (δ_E=95.3%) windows, but the deviation of amplitude spectra inside the B_{exc} is from 0 to -6 dB and from +0.2 to -6 dB, respectively (Paavle *et al*, 2010). The impact of the squared-sine windowing was almost the same as it of the Hanning window.

As a rule, windowing of the generated signal demands some additional power consumption and reduces the total energy-efficiency. However, in the case of very short signals this

drawback can be overcome using the look-up table, which stores the externally calculated values of windowed titlets and which is loaded into the FPGA (Min *et al*, 2011a).

4. Simulation examples

The following examples refer to the linear and quadratic sine-wave chirps and are the results of simulation using the modeling structure in Fig. 7. In all the cases, the chirp excitation from f = 0 to 100 kHz and amplitude A=1 V was implemented. The basic model of EBI was a 5-element impedance $\dot{Z}_1$, consisting of R_0=1 kΩ, R_1=200 Ω, R_2=100 Ω, C_1=30 nF, C_2=20 nF and having the following corner frequencies in the Bode diagram (see Fig. 2b): f_{p1}=2.9, f_{z1}=26.5, f_{p2}=45.2, and f_{z2}=79.6 kHz.

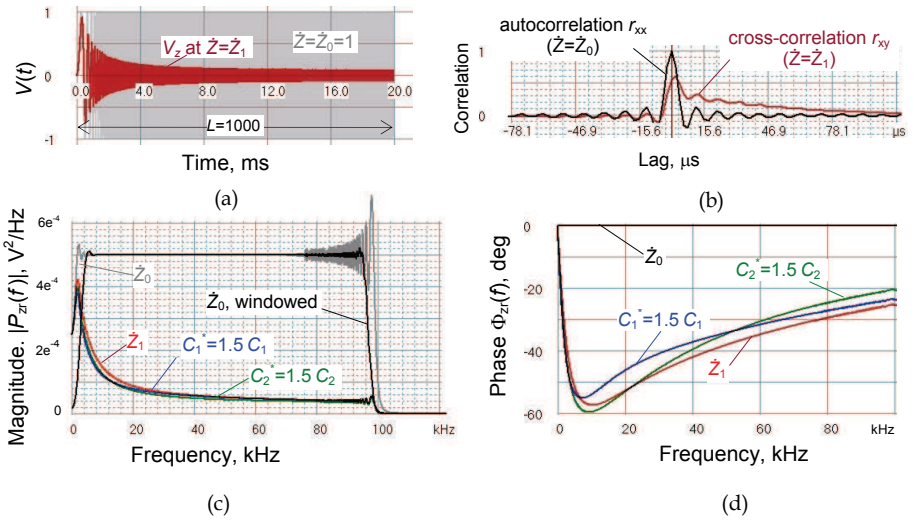

Fig. 16. Examples of the time-frequency analysis of the EBI (sine-wave chirp excitation with L=1000): (a) waveforms of excitation and response; (b) normalized correlation functions; (c, d) cross-power spectral density and phase spectra at variations of the EBI components

Fig. 16 demonstrates simulation results in the case of multi-cycle chirp excitation with pulse duration of T_{ch}=20 ms (1000 cycles). Fig. 16a shows the response voltage $V_z(t)$ on the background of the non-windowed excitation signal. Fig. 16b shows cross-correlation functions in a stretched time scale at the $\dot{Z}$= $\dot{Z}_1$, and at the unity value impedance $\dot{Z}$= $\dot{Z}_0$ =1 (in fact, the latter case corresponds to the autocorrelation function of the excitation signal). Results of the Fourier Transform of the CCF are shown in Figs. 16c and 16d, where one can watch the swing of spectral curves, if the capacitive components of EBI change by +50%. In addition, Fig. 16c demonstrates, how the boxcar-type windowing (here squared-sine Tukey window with the tapering time of $0.05T_{ch}$) reduces the influence of the Gibbs effect.

Intensive fluctuation of spectra, caused by the concurrent higher harmonics, can be more disturbing for signum-chirp excitation (see Figs. 10b, 12, and 13a). This problem can be diminished by proper selection of correlation parameters, e.g., the shorter t_{obs} with rougher frequency resolution smoothes spectrograms essentially (Paavle *et al*, 2008).

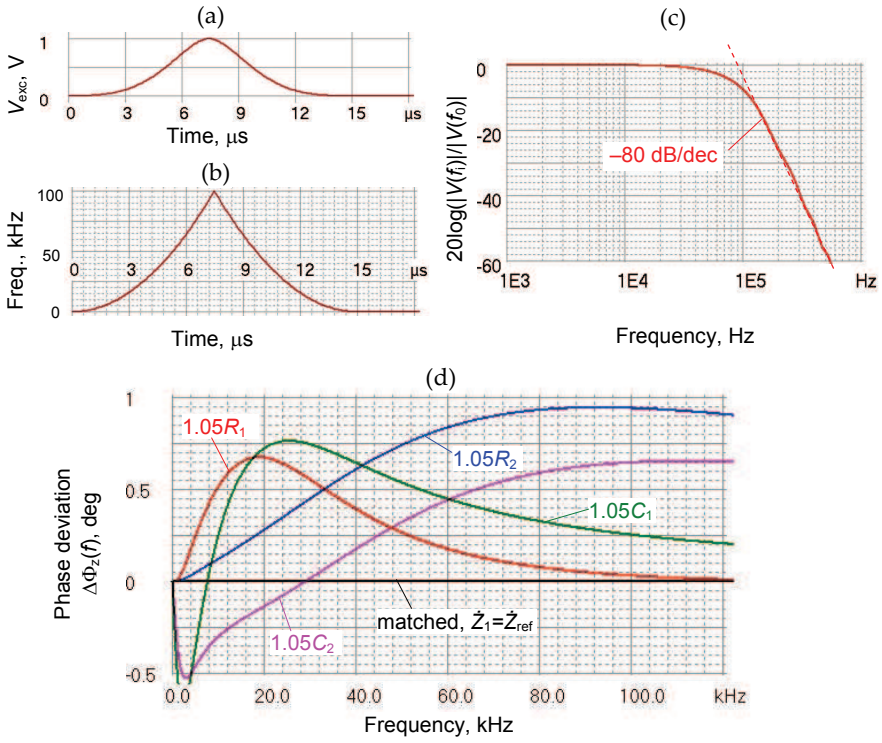

Fig. 17. The use of double quarter-cycle quadratic chirp excitation (L=¼, n=2, T_{ch}=2×7.5 µs, f_{st} =0, f_{fin}=100 kHz): (a) signal waveform; (b) variation of instantaneous frequency; (c) amplitude spectrum of the chirp pulse; (d) phase spectra at matched filtering ($\dot{Z}_{ref} = \dot{Z}_1$) and at changing of the EBI components +5%

For interpreting the variations of frequency responses, the phase spectra should be preferred. First, it is less affected by the spectral fluctuations. Secondly, the phase spectra enable to distinguish changing of object parameters somewhat more clearly than the amplitude ones – compare the respective curves in Figs. 16c and 16d. Nevertheless, substantially better resolution of the EBI for the diagnosing purposes can be achieved by using matched filtering, where instead of $\dot{Z}_{ref}$=1 in the reference channel, a predetermined $\dot{Z}_{ref} \approx \dot{Z}_x$ is used, approximately equal to the impedance $\dot{Z}_x$ under study (see Fig. 6). Joining matched filtering together with analysis of phase spectra allows applying the full scale of some degrees only and permits very good sensitivity for detection of small changes of the object parameters.

Simulation results in implementing of the bidirectional quarter-cycle quadratic chirp excitation for detection of tiny deviations of the EBI vector are presented in Fig. 17. The waveform of excitation pulse and the corresponding frequency run are shown in Figs. 17a and 17b, respectively. Fig. 17c depicts the normalized amplitude spectrum of the excitation signal and Fig. 17d manifests deviation of phase spectra, when the value of single components increases +5% over their initial quality.

Another advantage of the matched filtering is reducing the impact of additive noise, especially the impact of source noise $n_s(t)$. Fig. 18a depicts the noisy input signal, where the generated chirp is affected by the Gaussian noise with the zero mean and variance σ_N^2 – see Fig. 6. The source noise causes some error in the phase spectra at the higher frequencies (Fig. 18b). This error depends on the deviation of component parameters of the equivalent circuit (here C_1 was changed), and on the signal-to-noise ratio (SNR=P_{avg}/σ_N^2), but as a rule, the error remains small even at considerably high level of the source noise.

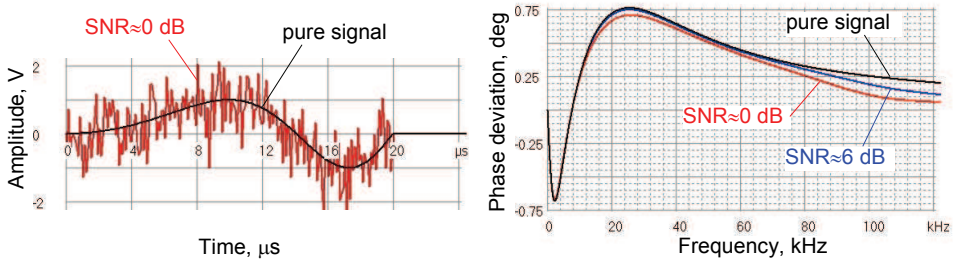

Fig. 18. Linear single-cycle chirp (T_{ch}=20 μs) at the presence of additive source noise: (a) noisy input signal; (b) spectra of phase differences at 1.05C_1 and at different input signal-to-noise ratio (SNR) levels

As the noise from object ($n_z(t)$ in Fig. 6) affects the cross-correlation procedure non-symmetrically, then suppression of noise effect is of importance and serves special attention even at the higher SNR values (Min *et al*, 2011b).

5. Conclusion

The advantages of using chirps as excitation signals in bioimpedance measurement are their wide and almost flat amplitude spectrum together with the independent scalability both in the time and frequency domain – we can choose the frequency range and duration of the excitation pulse almost independently from each other. These features enable to accommodate the generation of excitation signals with the expected properties of the object to be estimated comparatively simply.

It was shown that the shortening of chirp pulses retains the general benefits of chirps – their flat amplitude spectrum within the predetermined frequency range, which permits their implementation in energy-efficient measuring instruments. More than 90% of the generated excitation energy falls into the desired bandwidth even in the case of very short excitation pulses required for providing ultra quick measurement and analysis of dynamic objects. These requirements are obligatory for investigation of objects with rapidly changing parameters (e.g., for identification of fast moving bioparticles such as cells and droplets in high-throughput micro-fluidic systems), and in the devices, in which the low power consumption is important (e.g., wearable units and medical implants). However, shortening of chirp excitation and measurement time should not be excessive. It must be as short as possible to avoid significant impedance changes during the Fourier analysis, but as long as possible to enlarge the excitation energy and to obtain a better signal-to-noise ratio.

The described measurement method, based on the sequentially performed cross-correlation and Fourier Transform, enables the joint time-frequency spectral analysis of bioimpedance. As the time domain cross-correlation function includes the full information about the complex vector $\dot{Z}(\omega)$, only a single FFT-block is necessary for the Fourier analysis and the complete frequency domain determination of the object. Moreover, the cross-correlation procedure assures substantial suppression of noise introduced by the object.

Applying the modification of system architecture with the cross-correlation based matched filtering enables to avoid the impact of noise in much higher degree then a simple cross-correlation. In addition, such the matched filtering permits to increase the sensitivity of measurement, especially through the analysis of phase spectra. Identification and interpretation of relative deviations of the object parameters through the detected tiny phase shifts is of great importance, which in turn can give valuable information about the state and processes in the biological objects.

6. Acknowledgment

This work was supported by the European Union through the European Regional Development Fund, Estonian target-financed project SF0142737s06 and by Enterprise Estonia through the ELIKO Competence Center.

7. References

Barsoukov, E.; Macdonald, J. R. (Eds.) (2005). *Impedance Spectroscopy. Theory, Experiment, and Applications* (2nd ed.). John Wiley & Sons Ltd, Hoboken, New Jersey.

Darowicki, K.; Slepski, P. (2004). Determination of electrode impedance by means of exponential chirp signal. *Electrochemistry Communications*, No. 6, (June, 2004), pp.898-902.

Dwight, H. B. (1961). *Tables of Integrals and Other Mathematical Data*, The McMillan Company, New York, 1961.

Gawad, S.; Sun, T.; Green, N. G.; Morgan, H. (2007). Impedance Spectroscopy Using Maximum Length Sequences: Application to Single Cell Analysis. *Review of Scientific Instruments*, Vol. 78, No.5 (May, 2007).

Grimnes, S.; Martinsen, Ø. G. (2008), Bioimpedance and Bioelectricity Basics (2nd ed.), Elsevier-Academic Press, 2008.

McGhee, J.; Kulesza, W.; Henderson, I. A.; Korczynski, M. J. (2001). *Measurement Data Handling. Theoretical Technique.* Vol. 1, The Technical University of Lodz, Poland.

Min, M.; Parve, T. (2007). Improvement of Lock-in Electrical Bio-Impedance Analyzer for Implantable Medical Devices. *IEEE Trans. Instrumentation and Measurement*, Vol. 56, No. 3 (June 2007), pp.968-974.

Min, M.; Paavle, T.; Annus, P.; Land, R. (2009). Rectangular Wave Excitation in Wideband Bioimpedance Spectroscopy, *Proc. IEEE 4th Int. Workshop on Medical Measurements and Applications (MeMeA2009)*, Cetraro, Italy, May 29-30, 2009, pp.268-271.

Min, M.; Land, R.; Paavle, T.; Annus, P., Parve, T.; Trebbels, D. (2011). Broadband Spectroscopy of Dynamic Impedances with Short Chirp Pulses, *Physiological Measurement*, Vol. 32, No. 7 (July 2011), pp.945-958.

Min, M.; Paavle, T.; Ojarand, J. (2011). Time-Frequency Analysis of Biological Matter Using Short-Time Chirp Excitation. *Proc. of European Conference on Circuit Theory and Design (ECCTD2011)*, Linköping, Sweden, Aug. 29-31, 2011, pp.585-588.

Misaridis, T. X.; Jensen, J. A. (2005). Use of Modulated Excitation Signals in Medical Ultrasound. Part II: Design and Performance for Medical Imaging Applications, *IEEE Trans. on Ultrasonics, Ferroelectrics, and Frequency Control*, Vol. 52, No. 2 (Feb. 2005), pp. 192-207.

Müller, S.; Massarani, P. (2001). Transfer-Function Measurement with Sweeps, *J. Audio Eng. Soc.*, Vol. 49, No. 6, (June 2001), pp. 443-471.

Nahvi, M.; Hoyle, B. S. (2009). Electrical Impedance Spectroscopy Sensing for Industrial Processes, *IEEE Sensors Journal*, Vol. 9, No. 12 (Dec. 2009), pp.1808-1816.

Nebuya, S.; Brown, B. H.; Smallwood, R. H.; Milnes, P.; Waterworth, A. R.; Noshiro, M. (1999). Measurement of High Frequency Electrical Transfer Impedances from Biological Tissues. *Electronics Letters Online*, Vol. 35, No. 23 (1999), pp.1985-1987.

Paavle, T.; Annus. P. ; Kuusik, A. ; Land, R. ; Min, M (2007). Bioimpedance Monitoring with Improved Accuracy Using Three-Level Stimulus. *Proc. of European Conference on Circuit Theory and Design (ECCTD2007)*, Seville, Spain, Aug. 26-30, 2006, pp.412-415.

Paavle, T.; Min, M.; Parve, T. (2008). Using of Chirp Excitation for Bioimpedance Estimation: Theoretical Aspects and Modeling. *Proc. of 11th Baltic Electronics Conf. BEC2008*, Tallinn, Estonia, Oct. 6-8, 2008, pp. 325-328.

Paavle, T.; Min, M.; Ojarand, J.; Parve, T. (2010). Short-Time Chirp Excitations for Using in Wideband Characterization of Objects: an Overview. *Proc. of 12th Baltic Electronics Conf. (BEC2010)*, Tallinn, Estonia, Oct. 4-6, 2010, pp.253-256.

Parve, T.; Land, R. (2004). Improvement of Lock-in Signal Processing for Applications in Measurement of Electrical Bioimpedance. *Proc. of Estonian Acad. Sci. Eng.*, Vol. 10, No. 3 (Sept. 2004), pp.185-197.

Pliquett, U.; Gershing, E.; Pliquett, F. (2000). Evaluation of Fast Time-Domain Based Impedance Measurements on Biological Tissue. *Biomed. Technik*, Vol. 45 (Jan.-Feb. 2000), pp.6-13.

Rufer, L.; Mir, S.; Simeu, E.; Domingues, C. (2005). On Chip Pseudorandom MEMS Testing. *Journal of Electronic Testing: Theory and Applications*, Vol. 21, No. 3, pp.233-241.

Sanchez, B.; Vandersteen, G; Bragos, R.; Schoukens, J. (2011). Optimal Multisine Excitation Design for Broadband Electrical Impedance Spectroscopy. *Measurement Science and Technology*, IOP Publishing, 2011, Vol. 22, No. 11, 11 p.

Vaseghi, S. V. (2006)., *Advanced Digital Signal Processing and Noise Reduction*, (3rd ed.), John Wiley & Sons Ltd, Chichester, England, 2006.

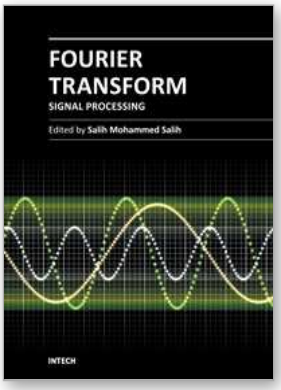

Fourier Transform - Signal Processing
Edited by Dr Salih Salih

ISBN 978-953-51-0453-7
Hard cover, 354 pages
Publisher InTech
Published online 11, April, 2012
Published in print edition April, 2012

The field of signal processing has seen explosive growth during the past decades; almost all textbooks on signal processing have a section devoted to the Fourier transform theory. For this reason, this book focuses on the Fourier transform applications in signal processing techniques. The book chapters are related to DFT, FFT, OFDM, estimation techniques and the image processing techqniques. It is hoped that this book will provide the background, references and the incentive to encourage further research and results in this area as well as provide tools for practical applications. It provides an applications-oriented to signal processing written primarily for electrical engineers, communication engineers, signal processing engineers, mathematicians and graduate students will also find it useful as a reference for their research activities.

How to reference
In order to correctly reference this scholarly work, feel free to copy and paste the following:

Toivo Paavle, Mart Min and Toomas Parve (2012). Aspects of Using Chirp Excitation for Estimation of Bioimpedance Spectrum, Fourier Transform - Signal Processing, Dr Salih Salih (Ed.), ISBN: 978-953-51-0453-7, InTech, Available from: http://www.intechopen.com/books/fourier-transform-signal-processing/aspects-of-using-chirp-excitation-for-estimation-of-bioimpedance-spectrum

INTECH
open science | open minds

InTech Europe
University Campus STeP Ri
Slavka Krautzeka 83/A
51000 Rijeka, Croatia
Phone: +385 (51) 770 447
Fax: +385 (51) 686 166
www.intechopen.com

InTech China
Unit 405, Office Block, Hotel Equatorial Shanghai
No.65, Yan An Road (West), Shanghai, 200040, China
中国上海市延安西路65号上海国际贵都大饭店办公楼405单元
Phone: +86-21-62489820
Fax: +86-21-62489821